Metabolomic Pattern of Childhood Neuroblastoma Obtained by [1]H-High-Resolution Magic Angle Spinning (HRMAS) NMR Spectroscopy

Alessio Imperiale, MD,[1,2]* Karim Elbayed, PhD,[3] François-Marie Moussallieh, Pharm D,[1,3] Agnès Neuville, MD,[4] Martial Piotto, PhD,[3,5] Jean-Pierre Bellocq, MD,[4] Patrick Lutz, MD,[6] and Izzie-Jacques Namer, MD, PhD[1,2]

Background. The aim of this preliminary study is to characterize by ^{1}H high-resolution magic angle spinning NMR spectroscopy (HRMAS) the metabolic content of intact biopsy samples obtained from 12 patients suffering from neuroblastoma (NB). ***Procedure.*** The biochemical NB profile was first compared to normal adrenal medulla. In a second step, the relationship between the tumor metabolic profile and the patients' clinical data was investigated. ***Results.*** A higher level of creatine, glutamine/glutamate, acetate and glycine characterized NB biopsies while healthy adrenal medulla tissue contained adrenaline and a larger amount of ascorbic acid. Adrenaline, which was undetectable in NB spectra, represented the metabolic signature of normal adrenal medulla. NB from patients younger than 12 months contained a higher level of acetate and lysine. Conversely, higher amounts of glutathione, glutamate, myo-inositol, glycine, serine and ascorbic acid were detected in NB samples belonging to younger children. Glutamine/glutamate, aspartate, creatine, glycine were characteristic of stage I–II NB. Acetate and creatine were characteristic of stage IV NB. Finally, a relatively higher amount of aspartate, succinate, and glutathione was detected in patients alive without active disease after a mean follow-up of 7 years whereas a higher concentration of acetate and taurine was characteristic of patients with worse prognosis. ***Conclusions.*** Our preliminary results suggest the existence of a complex metabolic reality in NB, probably representative of tumor behavior. However, the real impact of these promising results should be assessed by long-term prospective studies on a larger cohort of patients. Pediatr Blood Cancer 2011;56:24–34. © 2010 Wiley-Liss, Inc.

Key words: adrenal medulla; childhood malignancy; HRMAS; neuroblastoma; NMR; spectroscopy

INTRODUCTION

Neuroblastoma (NB) is one of the most common and lethal extracranial solid tumors of early childhood. According to the Automated Childhood Cancer Information System [1] the age-standardized incidence rate of NB in Europe in 1988–1997 was of 10.9 cases per million children, being highest in infants (52.6). NB arises from sympathetic nervous system tissues like adrenal medulla and paraspinal sympathetic nodes in the neck, chest and pelvis [2–5]. The clinical course of children with NB is highly variable, ranging from spontaneous regression or maturation into benign lesions to a rapid and dramatic metastatic spread [6,7]. The prognosis for patients with NB depends on several parameters such as the clinical stage of the disease, patient age at diagnosis and regional lymph node involvement for patients older than 1 year. Other potential prognostic variables include the site of the primary tumor as well as the catecholamine metabolite excretion ratio and the lactate dehydrogenase levels [6,7]. More recently, genetic and epigenetic prognosis factors have been identified such as the amplification of the *MYCN* oncogene, the tumoral cell ploidy as well as the loss of heterozygosity of 11q or 1p chromosome in tumor tissues [6].

Multimodal medical imaging plays a primary role in the management of children with NB. Computed tomography (CT), magnetic resonance (MR) and molecular imaging are successfully used for the assessment of tumor extension, both at primary staging and during follow-up [8–10]. Noninvasive imaging techniques also play a role, during the earlier phase of the treatment, in the selection of patients responding to conventional chemotherapy as opposed to the ones requiring alternative therapeutic strategies [11].

Magnetic resonance spectroscopy (MRS) can improve the understanding of the metabolic characteristics of the tissue that are directly related to tumor behavior. The potential value of in vivo and in vitro MRS has been previously documented in human and animal models of NB and other neuroectodermal tumors such as gliomas. Furthermore, MRS appears as a powerful non-invasive technique to investigate specific biochemical pathways in tumors and to predict the response to chemotherapy [12–17]. Unfortunately, the low spectral resolution of MRS only allows for the detection of a small number of molecules. Therefore, this technique might not be able to define with sufficient details the tumor characteristics. On the other hand, ^{1}H high-resolution magic angle spinning (HRMAS) is a nuclear magnetic resonance (NMR) technique that allows the characterization of the metabolic phenotype of intact cells, tissues and organs, from the analysis of intact tissue biopsy [18]. HRMAS NMR provides important biochemical information related to the regulation of specific gene transcripts that are altered in the genome of the tumor [19]. Multivariate statistical analysis applied to the whole NMR spectrum permits the assessment of the metabolic biomarkers responsible for the classification of the different tissues. To date, only a few applications of HRMAS NMR to pediatric brain and nervous system tumors have been described in the literature. Peet and coworkers showed the interest and the potential applications of HRMAS NMR in the evaluation of childhood NB in two recent studies by identifying not only the tumor metabolic profile, but also the specific biochemical fingerprint of MYCN-amplified and non-amplified tumor subtypes of NB cell lines [20,21].

---

[1]Biophysics and Nuclear Medicine Department, University Hospitals of Strasbourg, Strasbourg, France; [2]University of Strasbourg, CNRS LINC FRE 3289, Strasbourg, France; [3]University of Strasbourg, Institut de Chimie, CNRS UMR 7177, Strasbourg, France; [4]Pathology Department, University Hospitals of Strasbourg, Strasbourg, France; [5]Bruker Biospin, Wissembourg, France; [6]Pediatric Oncology Department, University Hospitals of Strasbourg, France

Conflict of interest: Nothing to declare.

*Correspondence to: Alessio Imperiale, Service de Biophysique et de Médecine Nucléaire, Hôpital de Hautepierre, 1, Avenue Molière, 67098 Strasbourg Cedex, France.
E-mail: alessio.imperiale@chru-strasbourg.fr

Received 20 October 2009; Accepted 30 April 2010

In the present study we have assessed, by means of HRMAS NMR, the metabolite profile of tumor tissue samples obtained from a cohort of 12 patients affected by NB. This work was performed with a twofold aim: (1) to define the NB biochemical profile with respect to normal adrenal medulla; (2) to establish the potential relationships existing between the NB metabolic profile and patients' clinical data such as: age at diagnosis, disease stage, and long term survival.

METHODS

Patients Population

Among all the patients affected with NB which were admitted in our Pediatric Oncology Department for primary staging, 12 children (9 boys, 3 girls; median age: 10 months; age range: 0.3–182 months) were retrospectively selected for this preliminary investigation according to the five following criteria: (1) final diagnosis of NB according to pathological criteria of the International Classification [22,23], (2) absence of both medical and surgical treatment before obtaining the tumor sample for HRMAS analysis, (3) tumor tissue sample acceptable to perform a correct HRMAS analysis (viable tumor/necrosis ratio), (4) tissue specimens collected immediately ($\leq$2 min) after surgery and snap-frozen in liquid nitrogen before storage at -80°C, and (5) absence of pollution of tissue samples by the histopathological fixing medium.

Among the 12 selected patients, 5 were younger than 12 months at diagnosis. The tumor developed in the retroperitoneum in 10 children. The adrenal gland was the primary tumoral site in seven of them. For the remaining two patients, NB originated from the thoracic or neck paraspinal sympathetic nodes. According to the International Neuroblastoma Staging System [24], seven patients were classified as stage 1, one patient as stage 2A and four patients as stage 4. Tumor was undifferentiated and poorly differentiated in respectively three and nine cases. *MYCN* gene amplification was determined by Southern blot analysis of the number of copies of the gene. Tumors with cells containing >10 copies of *MYCN* were considered as amplified. Among the 12 selected children, only one showed *MYCN* amplification. In our cohort, the clinical mean follow-up was 7 years (follow-up range: 1.5–13 years). During this period, three patients died, one is currently treated for a major relapse and eight are free of disease at the time of redaction of the article. Table I summarizes the main clinical characteristics of the selected patient cohort.

Human medullary adrenal tissue, which was obtained from subjects who underwent both nephrectomy and adrenalectomy, was used as normal control. Due to the retrospective nature of our study and to the difficulty in obtaining tissue sample from adrenal medulla that was properly stored after surgery, only three specimens (from three different patients) of normal adrenal medulla were available for HRMAS analysis.

Tissue Samples Collection and Preparation

Dissected tumor specimens were snap-frozen in liquid nitrogen immediately ($\leq$2 min) after surgery and then stored at -80°C. The amount of tumor tissue used for HRMAS analysis ranged from 15 to 20 mg. Each biopsy sample was introduced into a 30 µl disposable insert. Ten microliters of D_2O were added to the rotor to

TABLE I. Summary of the Clinical Characteristics of the Patient Population

Pt no.	Sex (M/F)	Age at diagnosis (months)	Disease stage (I–IV)	Primary tumor localization (HN/TH/AP)	Primary tumor origin (Adr/ExAdr)	Tumor differentiation	MKI (1–3)	MYCN (Am/NAm)	Survival status (CR/R/D)	Follow-up (years)
1	M	38	IV	AP	Adr	Undifferentiated	1	NAm	MR	3
2	M	36	IV	AP	Adr	Poorly diff.	1	NAm	D	2
3	F	23	IV	AP	Adr	Poorly diff.	1	Am	D	1.5
4	M	18	I	TH	ExAdr	Poorly diff.	1	NAm	CR	13
5	F	18	I	AP	Adr	Poorly diff.	2	NAm	CR	10
6	M	0.3	I	AP	ExAdr	Undifferentiated	1	NAm	CR	12
7	F	3	I	AP	Adr	Poorly diff.	2	NAm	CR	11
8	M	182	IV	AP	ExAdr	Poorly diff.	1	NAm	D	4
9	M	8	I	AP	Adr	Poorly diff.	1	NAm	CR	9
10	M	4	I	HN	ExAdr	Poorly diff.	1	NAm	CR	8
11	M	0.5	I	AP	ExAdr	Undifferentiated	1	NAm	CR	8
12	M	13	IIA	AP	Adr	Poorly diff.	2	NAm	CR	4

Pt, patient; HN, head-neck; TH, thorax; AP, abdomino-pelvis; Adr, adrenal; ExAdr, extra adrenal; diff., differentiated; MKI, mitosis-karyorrhexis index; MKI 1, low; MKI 2, intermediate; MKI 3, high; Am, amplified; NAm, not amplified; CR, complete remission; MR, major relapse; D, death.

provide a lock frequency for the NMR spectrometer. The exact weight of sample used was determined by weighting the empty rotor and the rotor containing the biopsy. The insert was stored at $-80°C$ and placed into a 4 mm ZrO_2 rotor just before the HRMAS analysis.

HRMAS: Technical Features

HRMAS spectra were recorded on a Bruker Avance III 500 spectrometer operating at a proton frequency of 500.13 MHz and equipped with a 4 mm double resonance (^{1}H, ^{13}C) gradient HRMAS probe. A Bruker Cooling Unit is used to regulate the temperature by cooling down the bearing air flowing into the probe. To minimize the effects of tissue degradation, all ex vivo spectra were acquired at a temperature of $4°C$. This value was calibrated exactly using a 100% methanol sample. All NMR experiments were conducted on samples spinning at 3,502 Hz in order to keep the rotation sidebands out of the spectral region of interest and to minimize sample degradation.

For each biopsy sample, a one-dimensional proton spectrum using a Carr-Purcell-Meiboom-Gill (CPMG) pulse sequence with a presaturation of the water signal was acquired as previously reported [25]. The inter-pulse delay between the $180°$ pulses of the CPMG pulse train was synchronized with the sample and set to 285 μsec ($1/\omega = 1/3,502 = 285$ μsec) in order to eliminate signal losses due to B_1 inhomogeneities [26,27]. The number of loop was set to 328 giving the CPMG pulse train a total length of 93 msec. Parameters for the CPMG experiment were: sweep width 14.2 ppm, number of points 32k, relaxation delay 2 sec, and acquisition time 2.3 sec. A total of 128 FID were acquired resulting in an acquisition time of 10 min. All spectra were recorded in such a manner that only a zero phase order correction was necessary to properly phase the spectrum. The FID was multiplied by an exponential weighing function corresponding to a line broadening of 0.3 Hz prior to Fourier transformation. Spectra were referenced by setting the lactate doublet chemical shift to 1.33 ppm.

In order to confirm resonance assignments, two-dimensional homonuclear and heteronuclear experiments were also recorded on eight samples immediately after the end of 1D spectra acquisition. 2D DIPSI2 spectra [28] were acquired with a 170 msec acquisition time, a 60 msec mixing time, a 14.2 ppm spectral width and a 1.5 sec relaxation delay. Thirty-two transients were averaged for each of the 512 increments during t1, corresponding to a total acquisition time of 8 h. Data were zero filled to a 2k × 1k matrix and weighted with a shifted square sine bell function prior to Fourier transformation. 2D ^{1}H-^{13}C HSQC experiments using echo-antiecho gradient selection for phase-sensitive detection were acquired using a 73 msec acquisition time with GARP ^{13}C decoupling and a 1.5 sec relaxation delay [29]. A total of 128 transients were averaged for each of 256 t1 increments, corresponding to a total acquisition time of 15 h. Two 1 msec sine-shaped gradient pulses of strength 40 and 10.05 G/cm were used in the experiment. Data were zero-filled to a 2k × 1k matrix and weighted with a shifted square sine bell function before Fourier transformation.

Statistical Analysis

HRMAS NMR signals were bucketed into integral regions of 0.01 ppm width (ppm range: 7.95–6.75 and 4.7–0.5) using the AMIX 3.8 software (Bruker GmbH, Rheinstetten, Germany)

and exported into SIMCA P (version 11.0, Umetrics AB, Umeå, Sweden). To accommodate the influence of metabolites present in both high and low concentrations, without emphasizing spectral noise, unit variance scaling was employed for all analyses.

Principal component analysis (PCA) and Partial Least Square Discriminant Analysis (PLS-DA) were conducted on 1D HRMAS CPMG NMR spectra of NB and normal adrenal medulla. PCA is an unsupervised statistical method commonly used to classify biological samples. However, PCA tends to generate a model with a large number of principal components, making the analysis of the variances along the different axis sometime difficult. PLS-DA is a supervised analysis procedure incorporating prior knowledge of class identity that maximizes the separation between groups, rather than explaining the maximum variation in the data. PLS-DA is able to differentiate two classes according to the pathological effect of interest using a relatively small number of components (2 or 3). Given the fact that the number of variables is usually much larger than the number of samples, there is clearly a risk of overfitting the data. However, when building a statistical PLS-DA model, the number of principal components is determined by cross-validation. This means that samples are kept out of model development and tested using the model. This procedure significantly limits the risks of overfitting by limiting the number of principal components. In the course of the PLS-DA analysis the class membership of every sample was iteratively predicted and the results were used to generate a goodness of the fit measure (Q^2) of the overall model where $Q^2 = (1 - PRESS/SS)$. PRESS is the predicted squared sum of error and represents the squared differences between observed and predicted Y values when the samples are kept out and SS is the residual sum of squares of the previous dimension. Even if the theoretical maximum is 1 for a perfect prediction, a $Q^2 > 0.5$ is generally considered as good predictor for PLS components. Finally, a circular validation was performed for each model. A model was considered as valid if the regression line obtained by random circular permutation of the Y values showed a negative slope and if all the estimated Q^2 were lower than the original one.

In our study, PLS-DA was initially performed on the whole set of variables in order to select those with a real discriminating power. Afterwards, a second PLS-DA analysis, based on the variables determined previously, was used to classify tissue samples according to the following factors: (1) histology (NB and control healthy adrenal), (2) patient age at diagnosis (below or above 1 year), (3) stage of disease (stage I–II or IV), and (4) patient outcome (long-term free disease survival or major relapse/death). Finally, a PCA analysis was performed on the whole biopsy cohort using only data points corresponding to the previously selected metabolites in order to validate the PLS-DA results by an unsupervised statistical technique.

RESULTS

NB and Healthy Adrenal Tissue

The mean 1D HRMAS CPMG spectra of both NB and healthy medullary adrenal tissue are presented in Figure 1. A representative 2D HSQC spectrum of the two types of tissues is presented in Figure 2. Metabolites were assigned using standard metabolite chemical shift tables available in the literature [30,31]. From the analysis of all NB and healthy control biopsies, 35 different metabolites were identified between 7.95–6.75 and 4.7–0.5 ppm (Table II).
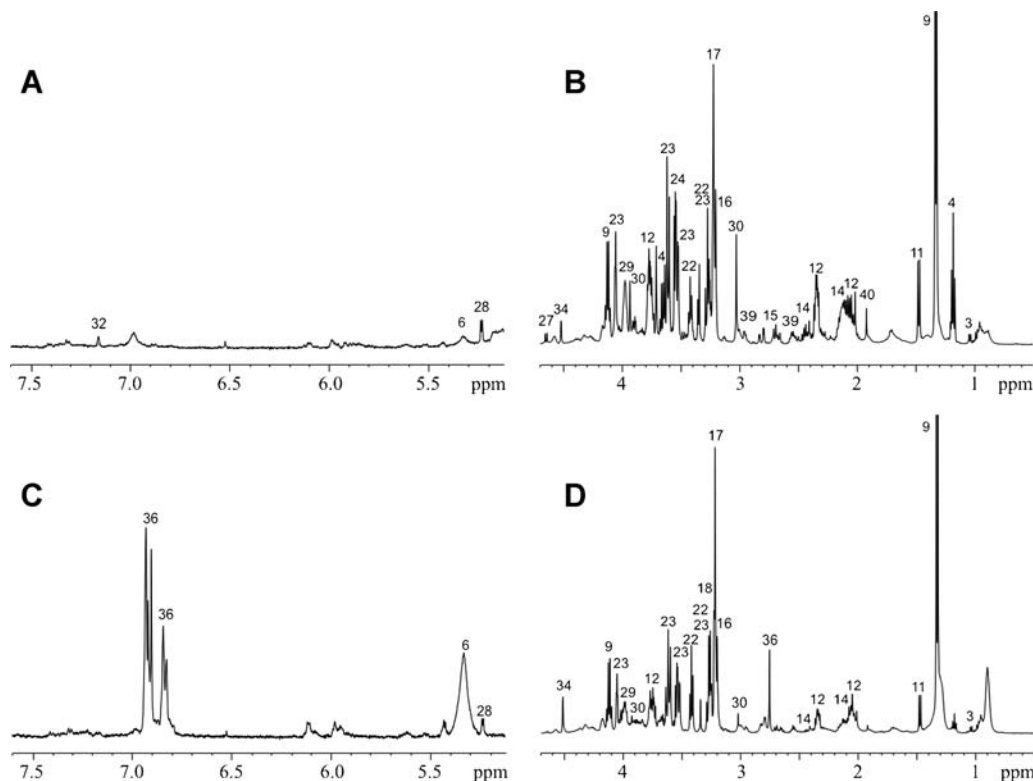
Fig. 1. Mean 1D ¹H CPMG HRMAS spectra of neuroblastoma (**A,B**) and healthy adrenal medulla (**C,D**) tissues. Partial metabolite assignment is indicated. The numbers refer to the metabolites listed in Table II. The metabolic content of healthy and cancerous biopsies can be directly compared since the intensity of each spectrum was normalized with respect to the weight of biopsy present in each sample.

These spectra show that NB are characterized by a higher level of creatine, glutamine/glutamate, acetate, and glycine. Correspondingly, healthy tissues contain adrenaline and a larger amount of ascorbic acid. The adrenaline complex, which is undetectable in all NB spectra (Figs. 1 and 2), represents the metabolic signature of normal adrenal medulla.

A PLS-DA analysis was performed on the CPMG data in the 7.95–6.75 and the 4.7–0.5 ppm range (12 NB and 3 normal adrenal medulla). The analysis generated a two-component PLS-DA model characterized by a faithful representation of the Y data ($R^2Y = 0.97$) and a good cumulative confidence criterion of prediction ($Q^2 = 0.76$). The score plot of the PLS-DA model showed a very clear separation of the two sets of biopsies. Indeed, the PLS-DA model revealed a statistically significant elevation of creatine, glutamine/glutamate, acetate, and glycine in NB compared to healthy tissues. Apart from a higher amount of ascorbic acid, the main metabolic signature of adrenal medulla consisted in the presence of adrenaline which was undetectable in all NB specimens.

A second two-component PLS-DA model was built using only the most discriminant metabolites previously determined (Fig. 3). The resulting PLS-DA model was characterized by the same R^2Y value (0.97) and a better cumulative confidence criterion of prediction ($Q^2 = 0.86$).

Following this classification process, a three component PCA analysis was performed on the whole biopsy cohort using only data points corresponding to creatine, glutamine/glutamate, acetate, glycine, ascorbic acid and adrenaline. The PCA model showed a differentiation between tumoral and control biopsies ($R^2X = 0.55$ and $Q^2 = 0.30$) (Fig. 3).

Patient Age at Diagnosis

According to the age of the patient at diagnosis, two groups were defined: children younger (n = 7) and older (n = 5) than 12 months. A PLS-DA analysis was performed on the CPMG data (4.7–0.5 ppm) obtained from the whole set of NB biopsies. The analysis generated a two components PLS-DA model showing an accurate representation of the data ($R^2Y = 0.96$) and a good cumulative confidence criterion of prediction ($Q^2 = 0.64$). A statistically significant elevation of glutathione, glutamate, myo-inositol, glycine, serine and ascorbic acid was detected in tissue samples belonging to the seven younger children. Conversely, a higher concentration of acetate and lysine was evidenced in the five patients older than 1 year.

A second PLS-DA model was built using only the most discriminant metabolites (Fig. 3). The resulting two components PLS-DA model was characterized by $R^2Y = 0.99$ and $Q^2 = 0.90$.

A two components PCA analysis was subsequently performed using only the data points corresponding to glutathione, glutamate, myo-inositol, glycine, serine, ascorbic acid, acetate, and lysine. PCA was able to differentiate, in an unsupervised manner, biopsies from younger (<1 year) and older patients (>1 year) ($R^2X = 0.53$ and $Q^2 = 0.2$). Figure 3 represents the score plot of the PCA model showing a clear separation of the two classes of biopsies.

Disease Stage and Patient Outcome

In our population, patients' disease stage at diagnosis was accurately correlated to prognosis. Indeed, three out of four stage IV

TABLE II. ^{1}H NMR Resonance Assignments of the Metabolites Present in Neuroblastoma and Healthy Human Adrenal Medulla

	Metabolites	Group	[1]H chemical shift (ppm)	[13]C chemical shift
1	Isoleucine	δCH_3	0.94	13.79
		γCH_3	1.01	17.29
		γCH_2	1.51	27.30
		αCH	3.65	62.34
2	Leucine	δCH_3	0.95	23.43
		$\delta' CH_3$	0.91	24.52
		γCH	1.70	—
		βCH_2	1.70	42.37
		αCH	3.73	56.06
3	Valine	γCH_3	0.98	19.16
		$\gamma' CH_3$	1.04	20.65
		βCH	2.30	31.94
4	Ethanol	CH_3	1.18	19.47
		CH_2OH	3.66	60.16
5	Fatty acids (a)	$(2)CH_2$	1.29	34.53
		$(1)CH_2$	1.31	25.36
6	Fatty acids (b)	$(2)CH_2$	2.03	27.35
		CH_2	2.80	28.16
		$(1)CH$	5.33	130.51
		$(2)CH$	5.33	132.20
7	Fatty acids (a) (b)	$(n)CH_2$	1.29	32.40
8	Fatty acids (c)	$(2)CH_2$	1.60	27.30
9	Lactate	CH_3	1.33	22.70
		CH	4.12	71.11
10	Lysine	γCH_2	1.43	24.21
		δCH_2	1.71	29.10
		βCH_2	1.89	32.56
		εCH_2	3.01	41.80
11	Alanine	βCH_3	1.48	18.81
		αCH	3.78	53.22
12	Glutamate	βCH_2	2.05	29.74
		γCH_2	2.34	35.95
		αCH	3.76	57.20
13	MethionineεCH_2	2.12	16.61	
14	Glutamine	βCH_2	2.14	—
		γCH_2	2.44	33.48
		αCH_2	3.77	—
15	Aspartic acid	$\beta CH_2(u)$	2.70	39.17
		$\beta CH_2(d)$	2.80	39.17
		αCH	3.90	54.93
16	Choline	$-N^+-(CH_3)_3$	3.21	—
		βCH_2	3.52	69.96
		αCH	4.06	58.27
17	Phosphorylcholine	$-N^+-(CH_3)_3$	3.22	56.52
		βCH_2	3.60	68.98
		αCH	4.16	60.60
18	Glycerophosphocholine	$-CH_2-NH_3^+$	3.23	—
		αCH_2	4.32	62.19
		βCH_2	3.69	68.50
		$CH_2\text{-}HPO_4(d)$	3.88	69.10
		CH_2OH	3.91	73.24
		$CH_2-HPO_4(u)$	3.95	69.10
19	Arginine	γCH_2	1.70	26.75
		βCH_2	1.92	30.15
		δCH_2	3.21	43.27
20	Taurine	$-CH_2-NH_3^+$	3.26	50.13
		$-CH_2-SO_3^-$	3.42	38.06
21	Proline	$\delta CH_2(u)$	3.32	48.83
		$\delta CH_2(d)$	3.41	48.83
		αCH	4.10	64.39
22	Scyllo-inositol	All Hs	3.35	76.32
23	Myo-inositol	C_5H	3.27	77.00

TABLE II. (*Continued*)

	Metabolites	Group	¹H chemical shift (ppm)	¹³C chemical shift
		C_1H, C_3H	3.54	73.84
		C_4H, C_6H	3.61	75.06
		C_2H	4.06	74.85
24	Glycine	αCH	3.56	44.09
25	Threonine	αCH	3.60	63.04
		βCH	4.24	68.67
26	Glycerol	1,3 CH_2OH(u)	3.56	65.09
		1,3 CH_2OH(d)	3.65	65.09
		–CH(OH)–	3.78	74.85
27	β-Glucose	C_4H	3.43	72.58
		C_3H, C_5H	3.47	78.44
		C_6H(u)	3.75	63.44
		C_6H(d)	3.89	63.44
		C_1H	4.65	—
28	α-Glucose	C_1H	5.23	—
29	Serine	αCH	3.84	59.12
		βCH	3.97	62.88
30	Creatine	CH_3	3.03	39.64
		CH_2	3.93	56.36
31	Asparagine	αCH	4.00	54.15
32	Tyrosine	αCH	3.92	58.72
		CH 3,5	6.87	118.50
		CH 2,6	7.16	133.37
33	Phenylalanine	CH 2,6	7.30	131.81
		C_4	7.37	131.49
34	Ascorbic acid	CH_2OH	4.02	72.12
		C_4H	4.52	—
35	Succinic acid	(α,β,CH_2)	2.40	—
36	Adrenaline	CH_3–NH	2.76	65.61
		C_4H	6.84	120.93
		C_3H	6.92	118.88
		C_6H	6.93	116.26
37	Uracil	C_5H	5.78	103.65
		C_6H	7.53	146.66
38	N-Acetyl aspartate	CH_3	2.04	24.65
		αCH	4.37	55.90
39	Glutathione	CH_2–CONH	2.54	33.79
		CH_2–SH	2.95	28.20
		CH–NH_2	3.78	46.03
40	Acetate	CH_3	1.92	25.97

Metabolites were assigned using standard metabolite chemical shift tables available in the literature [17,20].

children died, and one developed a major relapse during follow-up. Consequently, the statistical analysis was performed according to different criteria: (1) normal adrenal tissues versus NB specimens from stage I–II and stage IV children, in separate and independent manner; (2) NB specimens from dead or relapsing children (stage IV) versus NB specimens from free-disease patients after a mean follow-up of 9 years (stage I–II), reflecting both the overall survival and disease stage effect.

Healthy Adrenal and NB Stages I–II and IV

Two independent PLS-DA analysis (two components each) of the CPMG data applied to the 7.95–6.75 and the 4.7–0.5 ppm ranges were able to differentiate control tissues (n = 3) from stage I to II (n = 8) or stage IV (n = 4) NB samples, showing accurate representation of the data and good cumulative confidence criterion of prediction: (a) control versus stage I–II: $R^2Y = 0.90$,

$Q^2 = 0.80$; (b) control versus stage IV: $R^2Y = 0.96$, $Q^2 = 0.77$.

A statistically significant elevation of glutamine/glutamate, aspartate, creatine, glycine was detected in stage I–II NB samples. Acetate and creatine mainly contributed to the discrimination of stage IV NB from healthy control. Adrenaline remained the most specific metabolite for normal tissue characterization, associated to ascorbate, glycerophosphocoline and fatty acids.

PLS-DA and PCA models (two components each) were then built using only the most discriminant metabolites and the following promising results were achieved: (a) control versus stage I–II: $R^2Y = 0.99$, $Q^2 = 0.93$ for PLS-DA and $R^2X = 0.65$, $Q^2 = 0.33$ for PCA; (b) control versus stage IV: $R^2Y = 0.99$, $Q^2 = 0.89$ for PLS-DA and $R^2X = 0.77$, $Q^2 = 0.36$ for PCA.

Figure 4 represents the score plot of the PLS-DA and PCA models. A clear separation between the two classes of biopsies by both supervised and unsupervised approaches is indeed achieved.
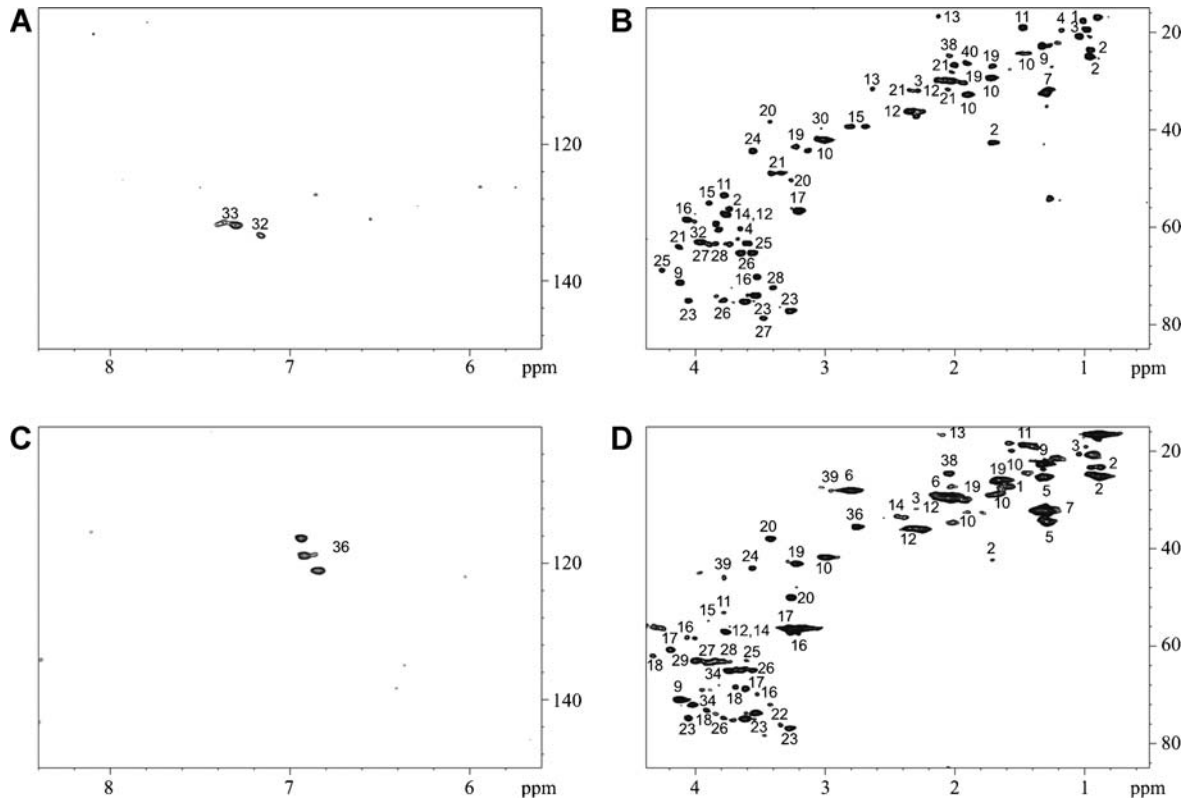
Fig. 2.   Representative 2D ^{1}H-^{13}C HSQC HRMAS spectra of neuroblastoma (**A,B**) and healthy adrenal medulla (**C,D**) tissues. Partial metabolite assignment is indicated. The numbers refer to the metabolites listed in Table II.

Patient Late Outcome

Based on patients' long-term survival (mean follow-up of 7 years), two groups were defined as follows: (a) patients who died or had a major relapse (n = 4) and (b) patients with complete remission (n = 8). A PLS-DA analysis (two components, R^{2}Y = 0.90, Q^2 = 0.30) was performed on the CPMG data (4.7–0.5 ppm region) obtained from the whole set of NB biopsies, showing a relative higher amount of aspartate, succinate, and glutathione in patients without active disease. Conversely, a higher concentration of acetate and taurine was present in the four patients with worse prognosis. A second PLS-DA model, which was created using only the most discriminant metabolites, was characterized by R^{2}Y = 0.90 and Q^2 = 0.62. A three components PCA analysis was successfully performed using only data points corresponding to aspartate, succinate, glutathione, acetate and taurine (R^{2}X = 0.67 and Q^2 = 0.20). PLS-DA and PCA results are graphically presented in Figure 4.

DISCUSSION

In this work, we have analyzed by HRMAS NMR tissue samples of childhood NB obtained by diagnostic biopsy from 12 untreated children. The first goal of this study was to characterize the metabolic profile of childhood NB. Although the metabolic fingerprint of NB has previously been studied using both in vivo and in vitro MRS and HRMAS NMR [12–17][20,21,32], the characteristics of NB were only assessed with respect to brain and nervous system tumors. In our study, we have compared childhood NB to healthy tissues that have the same neuroectodermal embryological origin as the adrenal medulla. This approach allowed for the characterization of the biochemical pattern of the physiological adrenergic tissue. Its specific signature is the presence of adrenaline whose resonances are particularly evident in the 7–6.5 ppm region of the NMR spectrum. The second aim of our study was to explore the potential relationships existing between the NB metabolite profile and the patients' clinical data such as the age at diagnosis, the disease stage and the long-term survival. To our knowledge, no previous work has reported such an exhaustive correlation study between HRMAS NMR data and clinical parameters of children with NB. Nevertheless, given the small number of samples, we must still consider the results of our work as preliminary.

Multivariate statistical analysis was applied to all the NMR spectra obtained from NB and healthy adrenal tissue. This type of analysis allows classifying the samples into two different groups according to their metabolic profile. The metabolites responsible for the classification appear clearly in such an analysis. It is necessary to stress that the discriminating power of each metabolite is linked to its relative difference in concentration between the two groups (i.e., NB vs. healthy control). Therefore, a metabolite present in low concentration in one group but completely absent in the other one will play a major role in discriminant analysis. Conversely, a metabolite detected in high concentration in both groups will be less significant in the clustering process (inconsistent relative difference).

The metabolic fingerprint of NB was characterized by general metabolic markers of malignancy such as choline-containing compounds, which are linked to an increased phospholipid turnover, but also by biochemical markers representative of fermentative processes and increased glycolytic activity such as lactate and
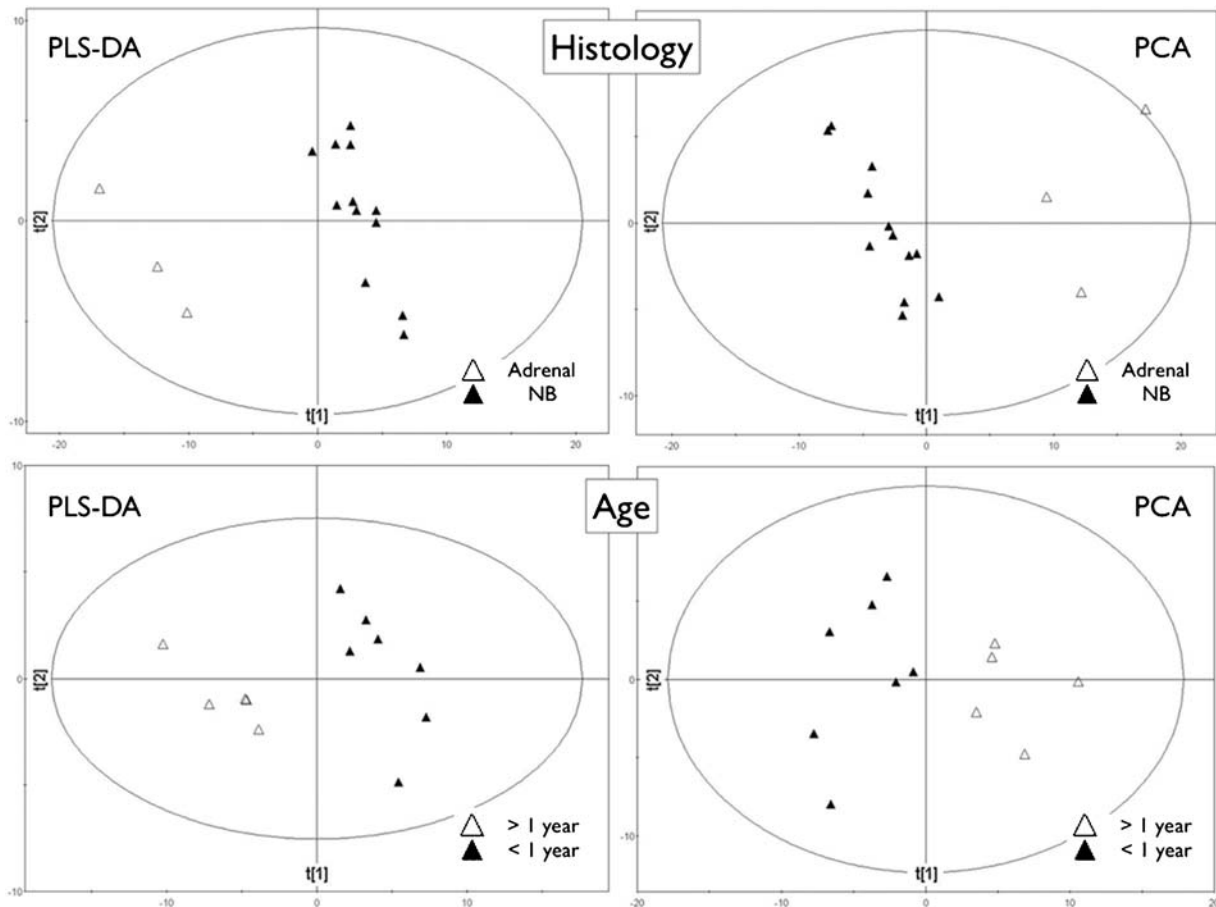
Fig. 3. PLS-DA and PCA models obtained when classifying neuroblastoma and healthy adrenal biopsies according to histopathological criteria (**upper panel**) and neuroblastoma biopsies according to patient age at diagnosis: older or younger than 1 year (**lower panel**).

glucose. The abundance of amino acids resonance peaks suggested an increase in amino acids production via non-oxidative pathways. The increased rate of protein degradation related to cell death, which is particularly evident in large and necrotic tumors, or the deregulation of the Krebs cycle, may explain the altered amino acid concentration observed in NB biopsies. Lipids, creatine, taurine, myoinositol, glycerol, glutamine/glutamate, and acetate were also present, playing an important complementary role in defining the metabolic profile of NB.

In 1995, Florian et al. [32] determined the metabolic characteristics of three types of human brain and nervous system tumors by high-resolution in vitro MRS and chromatographic analysis. Signals from leucine, isoleucine, glycine, valine, threonine, lactate, acetate, glutamate, and choline-containing compounds were similarly detected in meningiomas, glioblastomas, and NB. Intense signals from creatine were exclusively found in spectra obtained from perchloric extracts of NB cells. In our experiments, creatine was relatively more abundant in NB tissue than in control biopsies, especially in stage IV patients. Furthermore, creatine played a role in the statistical recognition of children with a bad prognosis.

In our study, the signals of the glutamate/glutamine complex were also present in NB tissue. A possible explanation is that some human NB cell lines are able to convert glutamate to GABA [33]. Roberts et al. [34] reported for the first time the association between the GABAergic system and the clinical outcome in human models

of NB. These authors showed that a lower expression of GABAergic system genes was associated with both older age at diagnosis and decreased survival. The effective relationship between the degree of GABA concentration and patient age should be assessed in long-term prospective studies using a larger cohort of patients.

The spectral fingerprint of NAA was also detected in HSQC and DIPSI2 spectra suggesting the presence of NAA in both NB and healthy control specimen. The origin from primordial neural crest cells may explain the detection of NAA in both NB and adrenal medulla samples. In normal condition, NAA is found mainly in healthy neuron and has been reported as a neuronal marker.

The metabolic profile of the normal adrenal medulla has not been previously assessed by HRMAS NMR. Our study shows that adrenaline is the specific metabolic signature of normal adrenal medulla (Figs. 1 and 2). Adrenaline resonances were undetectable in all NB spectra. Interestingly, both tyrosine and dihydroxyphenylalanine (DOPA), which are direct metabolic precursors in the adrenaline synthetic pathway, were identified in NB specimens. Thus, we could hypothesize a lower activity of dopamine β-hydroxylase and/or phenylethanolamine-N-transferase that are key role enzymes in adrenaline synthesis starting from tyrosine. In this context, the low cellular differentiation could account for the low adrenaline production and the consequent increase of intermediate metabolites.
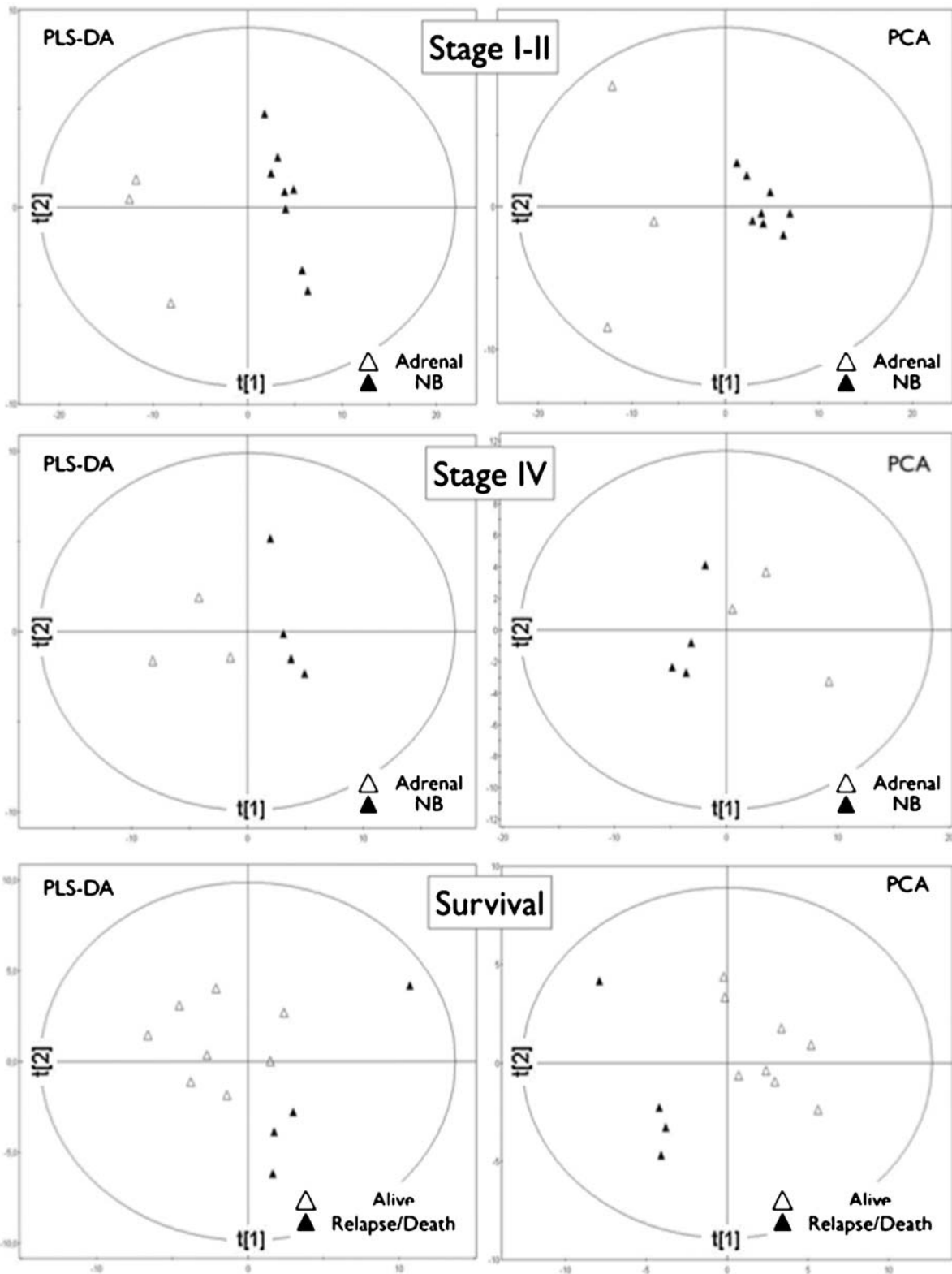
Fig. 4. PLS-DA and PCA models obtained when classifying neuroblastoma and healthy adrenal biopsies according to disease stage in separate and independent manner (**upper** and **middle panels**) and neuroblastoma biopsies according to patient long term survival: death/major relapse and complete remission after a mean follow-up of 9 years (**lower panel**).

In 2007, Peet et al. [20] reported the results of in vitro HRMAS investigations performed on cell suspension of 13 lines of NB possessing multiple genetic alterations. In their study, a specific metabolite profile associated with *MYCN*-amplified and non-amplified tumor subtypes was described. Phosphocholine and taurine concentration ratios relative to total choline were found to be significantly more elevated in the *MYCN*-amplified as compared to the *MYCN*-non-amplified cell lines, suggesting that choline and taurine molecular pathways could be potential therapeutic targets. Unfortunately, only one NB of our cohort showed *MYCN* amplification, thus *MYCN* was not included in the statistical analysis. According to our results, taurine and acetate concentrations are more elevated in NB, particularly in children older than 1 year at the time of diagnosis and in stage IV patients. Even if taurine is physiologically implicated in neurodevelopment [35], its role in NB pathophysiology remains undeterminate. The esterification of acetate to form acetyl coenzyme A (acetyl CoA) as a major precursor in beta-oxydation for fatty acid synthesis is believed to be the main mechanism of acetate incorporation in tumors. Nevertheless, alternative biochemical pathways of acetate intake or accumulation may include the Krebs cycle and the synthesis of cholesterol through citrate. Further studies using radiolabeled acetate could represent an interesting axis of research in NB animal models to assess metabolic responses to novel targeted drugs such as specific metabolic modulators.

Recently, Wilson et al. [21] identified the key differences in the metabolite profiles of pediatric glial and primitive neuro-ectodermal tumors by HRMAS NMR analysis. These authors provided an accurate biochemical characterization useful to improve our understanding of tumor molecular pathways, which are potential targets for drug development. According to previously published results obtained from the analysis of NB cell lines [20], Wilson and coworkers showed the presence of high taurine concentration in NB tissue, underlining its possible role in tumor development. The existence of high tissue heterogeneity in the same tumor, a major characteristic of human malignancy, could in theory reduce the accuracy of our HRMAS NMR results. However it has recently been reported that for NB, there is a smaller variability in metabolite concentrations within a given tumor than between different tumors [21]. This result pleads for a biochemical characterization of NB by HRMAS NMR.

The small number of samples and the lack of a prior hypothesis make however this study a very preliminary investigation. The metabolic profile of NB found in three patients who ultimately died cannot be considered as predictive of fatal issue. A larger cohort of patients will be absolutely necessary to confirm these first observations. In addition, the relative lack of tissue available for both high stage tumors and *MYCN* amplified tumors means that the most clinically important tumors with a particularly poor prognosis are not adequately represented.

In conclusion, our preliminary results suggest the existence of a complex metabolomic reality in NB, representative of tumor behavior and probably related to established clinical prognosis factors. However, the real impact of these interesting results should be assessed in long-term prospective studies of a larger cohort of patients.

ACKNOWLEDGMENTS

REFERENCES

1. Spix C, Pastore G, Sankila R, et al. Neuroblastoma incidence and survival in European children (1978–1997): Report from the Automated Childhood Cancer Information System project. Eur J Cancer 2006;42:2081–2091.
2. Miller RW, Young JL, Jr., Novakovic B. Childhood cancer. Cancer 1995;75:395–405.
3. Grovas A, Fremgen A, Rauck A, et al. The National Cancer Data Base report on patterns of childhood cancers in the United States. Cancer 1997;80:2321–2332.
4. Shimada H, Umehara S, Monobe Y, et al. International Neuroblastoma Pathology Classification for prognostic evaluation of patients with peripheral neuroblastic tumors: A report from the Children's Cancer Group. Cancer 2001;92:2451–2461.
5. Goto S, Umehara S, Gerbing RB, et al. Histopathology (International Neuroblastoma Pathology Classification) and MYCN status in patients with peripheral neuroblastic tumors: A report from the Children's Cancer Group. Cancer 2001;92:2699–2708.
6. Cotteril SJ, Pearson ADJ, Pritchard J, et al. Clinical prognostic factors in 1277 patients with neuroblastoma: Results of The European Neuroblastoma Study Group 'Survey' 1982–1992. Eur J Cancer 2000;36:901–908.
7. Adams GA, Shochat SJ, Smith EI, et al. Thoracic neuroblastoma: A Pediatric Oncology Group study. J Pediatr Surg 1993;28:372–377.
8. Hiorns MP, Owens CM. Radiology of neuroblastoma in children. Eur Radiol 2001;11:2071–2081.
9. Goo HW. Whole-body MRI of neuroblastoma. Eur J Radiol 2009;23 [Epub ahead of print].
10. Kushner BH. Neuroblastoma: A disease requiring a multitude of imaging studies. J Nucl Med 2004;45:1172–1188.
11. Taggart DR, Han MM, Quach A, et al. Comparison of iodine-123 metaiodobenzylguanidine (MIBG) scan and [18F]fluorodeoxyglucose positron emission tomography to evaluate response after iodine-131 therapy for relapsed neuroblastoma. J Clin Oncol 2009;27:5343–5349.
12. Lindskog M, Kogner P, Ponthan F, et al. Noninvasive estimation of tumor viability in a xenograft model of human neuroblastoma with proton magnetic resonance spectroscopy (1H MRS). Br J Cancer 2003;88:478–485.
13. Vaidya SJ, Payne GS, Leach MO, et al. Potential role of magnetic resonance spectroscopy in assessment of tumor response in childhood cancer. Eur J Cancer 2003;39:728–735.
14. Lindskog M, Spenger C, Jarvet J, et al. Predicting resistance or response to chemotherapy by proton magnetic resonance spectroscopy in neuroblastoma. J Natl Cancer Inst 2004;96:1457–1466.
15. Lindskog M, Spenger C, Klason T, et al. Proton magnetic resonance spectroscopy in neuroblastoma: Current status, prospects and limitations. Cancer Lett 2005;228:247–255.
16. Maris JM, Evans AE, McLaughlin AC, et al. 31P nuclear magnetic resonance spectroscopic investigation of human neuroblastoma in situ. N Engl J Med 1985;312:1500–1505.
17. Naruse S, Hirakawa K, Horikawa Y, et al. Measurements of in vivo 31P nuclear magnetic resonance spectra in neuroectodermal tumors for the evaluation of the effects of chemotherapy. Cancer Res 1985;45:2429–2433.
18. Nicholson JK, Wilson ID. Understanding 'global' systems biology: Metabonomics and the continuum of metabolism. Nature Rev Drug Discov 2003;2:668–676.

19. Griffin JL, Shockor JP. Metabolic profiles of cancer cells. Nat Rev Cancer 2004;4:551–561.
20. Peet AC, McConville C, Wilson M, et al. 1H MRS identifies specific metabolite profiles associated with MYCN-amplified and non-amplified tumour subtypes of neuroblastoma cell lines. NMR Biomed 2007;20:692–700.
21. Wilson M, Davies NP, Brundler MA, et al. High resolution magic angle spinning 1H NMR of childhood brain and nervous system tumours. Mol Cancer 2009;8:6.
22. Shimada H, Ambros IM, Dehner LP, et al. Terminology and morphologic criteria of Neuroblastic tumors: Recommendations by the International Neuroblastoma Pathology Committee. Cancer 1999;86:349–363.
23. Shimada H, Ambros IM, Dehner LP, et al. The International Neuroblastoma Pathology Classification (the Shimada System). Cancer 1999;86:364–372.
24. Look AT, Hayes FA, Shuster JJ, et al. Clinical relevance of tumor cell ploidy and N-myc gene amplification in childhood neuroblastoma: A Pediatric Oncology Group. J Clin Oncol 1991;9:581–591.
25. Piotto M, Moussallieh FM, Dillmann B, et al. Metabolic characterization of primary human colorectal cancers using high resolution magic angle spinning 1H magnetic resonance spectroscopy. Metabolomics 2009;5:292–301.
26. Elbayed K, Dillmann B, Raya J, et al. Field modulation effects induced by sample spinning: Application to high-resolution magic angle spinning NMR. J Magn Reson 2005;174:2–26.
27. Piotto M, Bourdonneau M, Furrer J, et al. Destruction of magnetization during TOCSY experiments performed under magic angle spinning: Effect of radial B1 inhomogeneities. J Magn Reson 2001;149:114–118.
28. Shaka AJ, Lee CJ, Pines A. Iterative schemes for bilinear operators; application to spin decoupling. J Magn Reson 1988;77:274–293.
29. Davis AL, Keeler J, Laue ED, et al. Experiments for recording pure absorption heteronuclear correlation spectra using pulsed field gradients. J Magn Reson 1992;98:207–216.
30. Martinez-Bisbal MC, Marti-Bonmati L, Piquer J, et al. 1H and 13C HR-MAS spectroscopy of intact biopsy samples ex vivo and in vivo 1H MRS study of human high grade gliomas. NMR Biomed 2004;17:191–205.
31. Wishart DS, Tzur D, Knox C, et al. HMDB: Human metabolome database. Nucleic Acids Res 2007;35:D521–D526 (Database issue).
32. Florian CL, Preece NE, Bhakoo KK, et al. Characteristic metabolic profiles revealed by 1H NMR spectroscopy for three types of human brain and nervous system tumours. NMR Biomed 1995;8:253–264.
33. Biedler JL, Roffler-Tarlov S, Schachner M, et al. Multiple neurotransmitter synthesis by human neuroblastoma cell lines and clones. Cancer Res 1978;38:3751–3757.
34. Roberts SS, Mori M, Pattee P, et al. GABAergic system gene expression predicts clinical outcome in patients with neuroblastoma. J Clin Oncol 2004;22:4127–4134.
35. Wharton BA, Morley R, Isaacs EB, et al. Low plasma taurine and later neurodevelopment. Arch Dis Child Fetal Neonatal Ed 2004;89:F497–F498.